Transaction B: Mechanical Engineering
Vol. 17, No. 1, pp. 41–52


SCIENTIA IRANICA

# Hydrodynamic Analysis of Non-Planing and Planing Hulls by BEM

**H. Ghassemi[1,*] and A.R. Kohansal[1]**

**Abstract.** *A three-dimensional, potential-based Boundary Element Method (BEM) is developed for the hydrodynamic analysis of non-planing and planing hulls in steady conditions. The method uses constant-strength doublet and source distributions over the body surface and source distributions on the free surface. Numerical computations are first applied to analyze the hydrodynamic characteristics and the free surface waves are generated by the mathematical non-planing model (Wigley hull), which is well known in ship hydrodynamics. The second type is a planing model, namely 4666, the experimental data of which were carried out by Clement and Blount [1]. Some numerical results of wave elevation, pressure distribution, lift and resistance are presented. Validations show that the computed results are in good agreement with experimental data and other numerical approaches.*

**Keywords:** *Wigley hull; Planing hull; Free surface; Pressure distribution; Resistance and lift coefficients.*

## INTRODUCTION

When a body moves near a free surface, its created wave pattern is one of the most interesting and more commonly evident phenomena. The energy spent in building this pattern comes from the work done by the body opposed to the wave resistance. A free surface allied with the water waves exists due to the gravity effect that is dealt to the pressure resistance component. As a result, the body is subjected to a resistance force known as the wave resistance, which is one of the most important resistance components in still water at the domain of a Froude number less than 0.5. When the Froude number is greater than 0.5, the hydrodynamic condition is changed and induced dynamic pressure is caused to lift up the body. Therefore, it passes the hump condition, gets a ride on the free surface and the wave effect is diminished [2].

Generally, resistance of the non-planing hull is categorized into two main components, i.e. wave making resistance and viscous resistance (form and frictional resistance), while for the planing hull, resistance components are frictional resistance, induced dynamic pressure resistance and spray resistance. The numerical prediction of hull resistance is very difficult, but it has less cost than experiment measurement. This actuality expresses the attempts involved in developing numerous theoretical approaches to evaluate resistance components accurately. This research work is divided into two parts. The first part is concentrated on the wave pattern and resistance of the non-planing hulls and the second part is focused on the dynamic pressure (induced lift and resistance) and spray resistance of the planing hulls.

The prediction of the wave pattern and resistance of a non-planing hull (Wigley) has challenged mathematicians and hydrodynamicists for over a century. The Boundary Element Method (BEM) establishes the basis for the majority of computational algorithms developed in recent years. This method may be classified into two categories. The first one uses the Kelvin wave source as the elementary singularity. The main advantage of such a scheme is the automatic satisfaction of the radiation condition. The theoretical background of this method was reviewed by Wehausen [3], while computational aspects can be found in the literature and in a series of wave resistance DTNSRDC Workshops edited by Noblesse and McCarthy [4]. The second category of BEM schemes uses the Rankine source as the elementary singularity. This procedure was first presented by Dawson [5]. Since then, it has

1. *Department of Marine Technology, Amirkabir University of Technology (AUT), Hafez Ave., Tehran, 15875-4413, Iran.*
*. *Corresponding author. E-mail: gasemi@aut.ac.ir*

*Received 11 March 2009; received in revised form 16 September 2009; accepted 15 November 2009*

been applied widely as a practical method and many improvements have been made to account for nonlinear wave effects. The Finite Element Method (FEM) has also been occasionally used to solve the free-surface potential flow problem in two- and three-dimensional domains [6]. Also, other work has been carried out using boundary element methods to deal with free-surface flows [7-12].

The need for an increase in the speed and payload of marine transportation has led to many research developments on High Speed Marine Vehicles (HSMVs). A planing craft is a HSMV, which may generate lift force by a well-designed hull. Numerical modeling of this problem is an important subject in ship design and naval architecture. Experiments have shown that the deadrise angle and the well-designed bottom shape of the hull are very important in planing crafts. The effect of the deadrise angle on hydrodynamic force, impact loading on the hull and high planing efficiency has led to a rational deadrise angle between $10° \leq \bar{\beta} \leq 15°$. Although the low deadrise angle and chine enhance the seakeeping performance, they may instigate other insufficiency problems like more slamming and porpoising (i.e. combined heaving and pitching instability). The form of stern is another aspect that is important in craft design. The transom stern is a common choice used in planing crafts. A number of advantages of this stern type are weight reduction, manufacturing efficiency and a possible resistance decrease in the speed range of craft operation.

Prediction of the resistance of a planing hull should be carried out in the first part of the designing process in order to estimate the required power for the propulsor and main engine. In past years, numerous experimental experiences have been performed by many researchers. Savistky [13] has made a great contribution to the understanding and modeling of a planing hull. He developed regression formulas based on prismatic hull form model tests to estimate the hydrodynamic forces. Clement and Blount [1] conducted an extensive set of model tests on a systematic series (Series 62 model 4666). This work remains one of the definitive sources of planing hull empirical information. Katayama et al. [14] performed resistance tests on prismatic planing hulls at various speeds and reported lift, resistance and moment coefficients.

From the numerical point of view, naval architects continue to improve the efficiency of computational tools to analyze high-speed planing hulls. Several valuable methods, using various computational techniques, have been developed in the past two decades. Lai and Troesch [15] applied a vortex lattice method to the planing body using the slender body theory. Zhao et al. [16] introduced the strip theory for steady planing in calm water. Savander et al. [17] used the boundary value problem for steady planing surfaces and obtained reliable relations between the perturbation potential and vortex distribution. Recently, Xie et al. [18] reported a study of the hydrodynamic problem of a 3-D planing surface using the vortex theory and the finite element approach. Rahmanian [19] applied the BEM for the hydrodynamic analysis of a planing hull and obtained the induced hydrodynamic lift and resistance in the steady condition. Hydrodynamic analysis of the planing hull at high Froude numbers was performed by Wang and Rispin [20] and Cheng and Wellicome [21]. Sadathusseini et al. reported the numerical simulation of free-surface waves and wave induced separation for the surface piercing hydrofoil of the NACA0012 section [22]. Recently, the combined method of a numerical and practical approach for hydrodynamic predictions of planing crafts has been executed by Ghassemi and Ghiasi [23], also Ghassemi et al. [24] addressed a nonlinear free surface boundary condition for the submerged lifting and non-lifting bodies using BEM.

The objective of this paper is to continue the development of a three-dimensional potential-based BEM for the hydrodynamics analysis of non-planing and planing hulls. Numerical results include pressure distributions, wave elevation, lift and resistance. It is shown that the results obtained by the present method are in good agreement with other numerical and experimental data.

## MATHEMATICAL FORMULATIONS

Let us consider a closed computational domain $\Omega$ with boundary $S$ and the unit normal vector $\hat{n}$ to $S$, being oriented into $\Omega$, as depicted in Figure 1. A Cartesian coordinate system, $o-xyz$, is established as the reference frame, with the origin fixed on the mean free surface as illustrated in Figure 2. The horizontal and vertical axes, $ox$ and $oz$, are along and at a right angle to the direction of motion. The origin, $o$, is taken as the base plane at transom. The body is moving with a constant speed $V_S$ in the $x$-direction on a calm water surface.

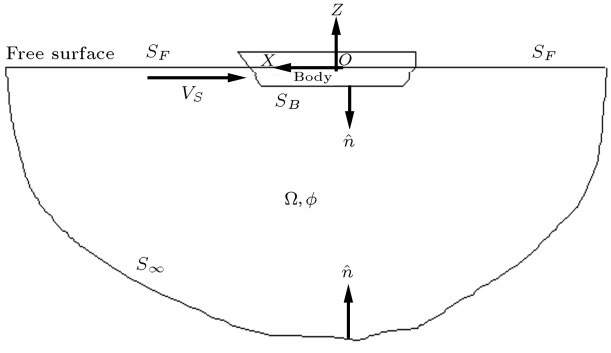


**Figure 1.** Application of Green's theorem for the general body.

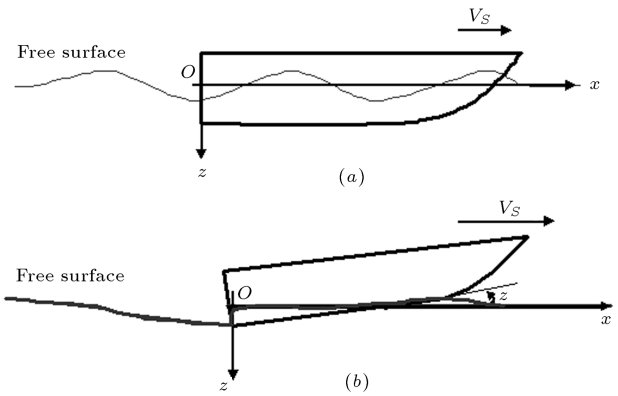


**Figure 2.** Coordinate system for planing and non-planing hulls.

Traditional ideal flow assumptions that ignore the effect of viscosity and compressibility are utilized. The double-body potential consists of inflow potential and flow due to the presence of the body. Total velocity potential $\Phi(x, y, z)$ is expressed as:

$$\Phi(x, y, z) = \phi_\infty(x, y, z) + \phi(x, y, z), \tag{1}$$

where $\phi_\infty(x, y, z) = \vec{V}_S.\vec{x}$ is incoming velocity potential, $\vec{x}$ is the position vector and $\phi(x, y, z)$ is the velocity potential due to interaction between the inflow potential, the body and the free surface. So, total potential can be written as follows:

$$\Phi(x, y, z) = \vec{V}_S.\vec{x} + \phi(x, y, z). \tag{2}$$

Both total and perturbation velocity potentials satisfy the Laplace equation in domain $\Omega$:

$$\nabla^2\Phi = \nabla\phi = 0. \tag{3}$$

### Boundary Conditions

A boundary value problem can be constructed by identifying boundary conditions on the boundary $S_B \cup S_F$ as follows:

i. Flow tangency condition on the body surface $S_B$: The normal component of the velocity on the hull surface must be zero.

$$\frac{\partial\Phi}{\partial n} = 0 \Rightarrow \frac{\partial\phi}{\partial n} = -\vec{V}_S.\vec{n} \quad \text{on} \quad S_B, \tag{4}$$

where $\vec{n} = n_x\hat{i} + n_y\hat{j} + n_z\hat{k}$ denotes the unit normal vector to the boundary, defined as positive when pointing into the fluid region.

ii. Radiation condition: There is no perturbation velocity in the far field upstream:

$$\Phi(x, y, z) \to x\vec{V}_S, \quad \text{far away upstream.} \tag{5}$$

Free surface boundary condition: the boundary conditions on the free surface are the Kinematic Free Surface Boundary Condition (KFSBC) and the Dynamic Free Surface Boundary Condition (DFSBC).

$$\begin{cases} \frac{\partial\Phi}{\partial x}.\frac{\partial\eta}{\partial x} + \frac{\partial\Phi}{\partial y}.\frac{\partial\eta}{\partial y} - \frac{\partial\Phi}{\partial z} = 0 & \text{on} \quad z = \varsigma, \\ g\eta + \frac{1}{2}(\nabla\Phi.\nabla\Phi - U^2) = 0 & \text{on} \quad z = \varsigma, \end{cases} \tag{6}$$

Consequently, the combined free surface boundary condition is defined as follows:

$$g\frac{\partial\Phi}{\partial z} + \nabla\Phi.\nabla\left(\frac{1}{2}\nabla\Phi.\nabla\Phi\right) = 0 \quad \text{on} \quad z = \varsigma, \tag{7}$$

where $g$ is gravitational acceleration. The boundary value problem formulated above is nonlinear, due to the free surface boundary condition and the unknown position of the corresponding boundary. The fully non-linear problem can be solved iteratively, or solved with a linearized free surface condition. Dawson [5] suggested a double body flow as the base flow to linearize the free surface condition. Linearized forms of free surface conditions have also been considered in this work. In the Neumann-Kelvin problem, the flow is linearized, with respect to the uniform forward speed $\vec{V}_S$. The following linearized free surface equation can be obtained as:

$$(\phi)_{xx} - K_0\Phi_z = 0 \quad \text{on} \quad S_F, \tag{8}$$

where $K_0 (K_0 = g/V_S^2)$ is the wave number. The flow potential $\phi$ is typically computed by a uniform free surface condition and the wave elevation is next obtained explicitly by the dynamic condition, whereas in the diffraction problem, the kinematic and dynamic conditions are generally implemented separately. To compute the free surface boundary condition $\phi_x$ can be calculated by a four-point upwind difference scheme.

iii. Far field condition: No disturbances are for the far field region, while the potential is bounded for far downstream as the radiation condition:

$$\lim|\nabla\phi| = 0, \quad \text{when} \quad r \to \infty, \tag{9}$$

iv. Kutta condition at the transom stern (special boundary condition for planing hull crafts): A Kutta condition should be satisfied at the trailing edge of the transom stern (Figure 2b). It means that the flow should be separated at the edge of the transom and can be expressed as follows:

$$\left|\frac{P_{\text{TE}} - P_{\text{atm}}}{P_{\text{atm}}}\right| < \varepsilon, \tag{10}$$

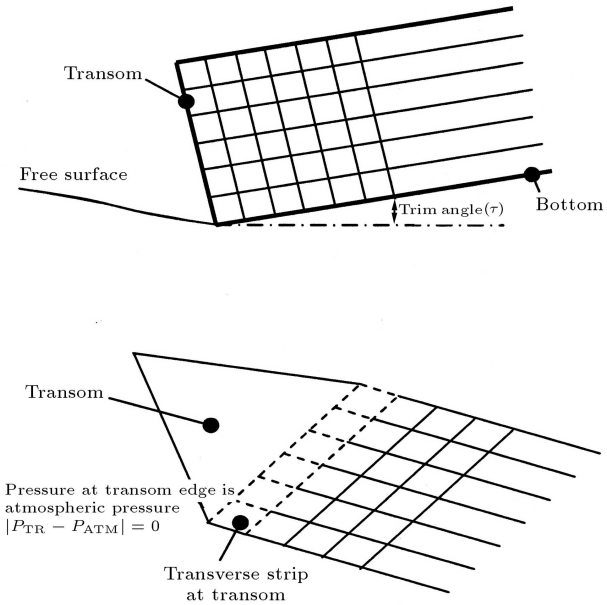


**Figure 3.** Transom stern configuration and boundary condition.

where $P_{\mathrm{TE}}$ and $P_{\mathrm{atm}}$ indicate the pressure values at the Transom Edge (TE) and atmospheric pressure, respectively (Figure 3). The drying process of a transom stern has been known to be a function of many variables, such as draft Froude number $(F_T)$ breadth to draft ratio $(B/T)$, buttock/trim angle and deadrise angle. However, in the planing condition, the transom is fully dried or ventilated. In order to develop an expression for potential derivation at the transom edge, the corresponding wave elevation in linearized form can be obtained as:

$$z = \eta(x,y) = \frac{V_S}{2g}\left[\frac{\partial\phi}{\partial x}\right]. \tag{11}$$

Since the separation should be occurred at the transom, it can be written as:

$$\eta = h = \frac{1}{2g}\left[V_S.\phi_X\right]. \tag{12}$$

Then:

$$\phi_x = \frac{2gh}{V_S}. \tag{13}$$

Potential $\phi$ is calculated by the boundary element method, which is based on Green's identity. In general, the boundary surface includes the body surface $(S_B)$ and the free surface $(S_F)$. Thus, the perturbation potential $\phi$ is given by the following integral expression, with points $Q$ (source point) on $S$ and $P$ (field point) in domain $\Omega$:

$$4\pi E\phi(P) = \int_{S_B}\left[\phi(Q)\frac{\partial G}{\partial n} - \frac{\partial\phi(Q)}{\partial n}G\right]dS - \int_{S_F}\left[\frac{\partial\phi(Q)}{\partial n}G\right]dS, \tag{14}$$

where $\frac{\partial}{\partial n}$ is normal derivative in respect to point $Q$ and $E$ is a solid angle that can be defined as follows:

$$E = \begin{cases} 1/2 & \text{for} \quad P \text{ on } S_B, \\ 1 & \text{for} \quad P \text{ on } S_F. \end{cases} \tag{15}$$

$G$ is Green's function, which might be expressed in the form $G = 1/r + 1/r'$. Here, $r$ is the distance between field point $P$ and source point $Q\left(r = \sqrt{(x-\xi)^2 + (y-\eta)^2 + (z-\zeta)^2}\right)$ and $r'$ is the distance between field point $P$ and the image of the source point relative to the mean free surface $\left(r'_{pq} = \sqrt{(x-\xi')^2 + (y-\eta')^2 + (z-\zeta')^2}\right)$ where $(\xi,\eta,\zeta)$ and $(\xi',\eta',\zeta')$ are coordinates of point $q$ and $q'$ respectively.

## NUMERICAL IMPLEMENTATION

### Discretized Formula

To obtain an approximate solution for integral Equation 14, the wetted body surface and free surface are discretized into quadrilateral elements. The discretized form of integral Equation 14 for the wetted surface of the body can be expressed as:

$$4\pi E\phi(P_i) = \sum_{\substack{j=1 \\ (i\neq j)}}^{N_B}\phi(Q_j)[DB_{ij}] - \sum_{j=1}^{N_B}\left(\frac{\partial\phi(Q)}{\partial n}\right)_j[SB_{ij}] - \sum_{j=1}^{N_F}\left(\frac{\partial\phi(Q)}{\partial n}\right)_j[SF_{ij}], \quad P_i \in S_B, \tag{16}$$

where:

$$DB_{ij} = \int_{S_B}\frac{\partial G_{ij}}{\partial n}dS_j, \quad SB_{ij} = \int_{S_B}G_{ij}dS_j, \quad SF_{ij} = \int_{S_F}\frac{1}{r_{ij}}dS_j, \tag{17}$$

and $N_B$ and $N_F$ are the number of elements on the wetted hull surface and free surface, respectively. The wetted surface adjustment is obtained through an iterative procedure. The velocity component $(\partial\phi/\partial n)$

is known on the body surface from Equation 4, while it is unknown on the free surface. Due to the linearized free surface condition, it can be defined as $\partial\phi/\partial n = -\partial\phi/\partial z = -\sigma$. The influence coefficients $(DB_{ij}, SB_{ij}, SF_{ij})$ are calculated by a numerical procedure. The matrix form of Equation 16 can be written as:

$$\begin{bmatrix} A & B \\ C & D \end{bmatrix} \cdot \begin{bmatrix} \{\phi\}_{N_B\times 1} \\ \{\sigma\}_{N_F\times 1} \end{bmatrix} = \begin{bmatrix} R \\ S \end{bmatrix}, \tag{18}$$

where:

$$A = [\delta - DB]_{N_B\times N_B},$$

$$B = [SF]_{N_B\times N_F},$$

$$C = [DB_{xx}]_{N_F\times N_B},$$

$$D = [-K_0\delta + SF_{xx}]_{N_F\times N_F},$$

$$R = [SB]_{N_B\times N_B}.\{-\vec{V_S}.\hat{n}\}_{N_B\times 1},$$

$$S = [SB_{xx}]_{N_F\times N_B}.\{-\vec{V_S}.\hat{n}\}_{N_B\times 1}. \tag{19}$$

Here, $\delta_{ij}$ is the Kronecker delta function, and the second derivative of the influence coefficients $(DB_{xx}, SB_{xx}, SF_{xx})$ are computed by a four-point finite difference operator. Also, a four-point upstream operator is introduced to satisfy the condition of no waves propagating upstream [4]. The total number of unknowns are $N_B + N_F(= N_T)$. $N_B$ is the number of unknown potential $(\phi)$ on the wetted body surface and $N_F$ is the number of unknown velocity components $(\sigma)$ on the free surface.

A formal solution of the matrix Equation 17 may be given by the direct solution methods of $LU$ decomposition or Gaussian elimination. Once perturbation potential $\phi$ is found, the induced velocity may be determined by the derivative of the perturbation potential, $\vec{v}_t = \nabla\phi$.

## Semi-Empirical for the Spray Resistance Computations

The spray phenomenon is the impact of a body with still water, which generates "upwash" at the bow. It is very difficult to recognize the characteristics of the spray to be calculated continuously by BEM. Therefore, an additional technique is required to consider this component. Savitsky et al. [25] determined spray drag in a performance prediction method for high-speed planing hulls. He proposed the following relationship between the wetted length, trim angle and deadrise angle:

$$L_K - L_C = \frac{B}{\pi}\frac{\tan\beta}{\tan\tau}, \tag{20}$$

where $L_K$ is keel wetted length, $L_C$ is chine wetted length, $B$ is hull breadth and $\beta$ and $\tau$ are deadrise and trim angle, respectively. Recently, Bowles and Denny [26] have presented an analytical model tool for predicting the water surface disturbance in close proximity to the bow of a planing hull, by the following equation:

$$L_K - L_C = \frac{B}{2}\frac{\tan\beta}{\tan\tau}\frac{1}{\left(\frac{1}{1+\tan(\beta)\tan(\beta/2)}\right)^{1/2}+1}. \tag{21}$$

The hull is assumed to run in steady state in calm water, i.e. with constant speed $V_S$, draft and trim angle $\tau$. The flow velocity component normal to the keel is $U = V_S\sin\tau$. The principal characteristics in the chine-dry region is illustrated in section $E-E$ (Figure 4). It is shown that the water surface is deformed and the pile-up is close to the hull. At the spray root, i.e. the intersection between the piled-up water line and the hull, a spray-jet is formed. The peak of the hydrodynamic pressure distribution relates to the formation of the jet. In the chine-wet region (section $F-F$), the sideway flow separates at the sharp chine where the hydrodynamic pressure adjusts to atmospheric pressure.

The hydrodynamic pressure of the spray is proportional to the geometrical configuration of the hull, such as the deadrise, the trim and the chine wet/dry regions and operation conditions, such as the speed and the water wave. In the present paper, the following practical method is utilized to determine spray resistance. The spray surface may be approximated as follows:

$$A_{\text{Spray}} = K_1(L_K - L_C)B/\cos\beta, \tag{22}$$

where $K_1$ is a constant value that depends on the hull speed and is given as follows:

$$K_1 = \begin{cases} 0.2 & \text{if} \quad Fn_\nabla < 3 \\ 0.4 & \text{if} \quad 3 \le Fn_\nabla < 5 \\ 0.7 & \text{if} \quad Fn_\nabla \ge 5 \end{cases} \tag{23}$$

Then, the pressure due to the spray can be calculated by the following equation:

$$P_S = K_2.P(\text{at bow of the keel}), \tag{24}$$

where:

$$K_2 = \begin{cases} 2 & \text{if} \quad b(y) < 0.5\ B \\ 1.5 & \text{if} \quad 0.5\ B \le b(y) < 0.9\ B \\ 1.2 & \text{if} \quad 0.9\ B \le b(y) \le B \end{cases} \tag{25}$$

and $P$ is the pressure obtained from Equation 28 at the nearest element to the spray root and $B$ and $b(y)$ are

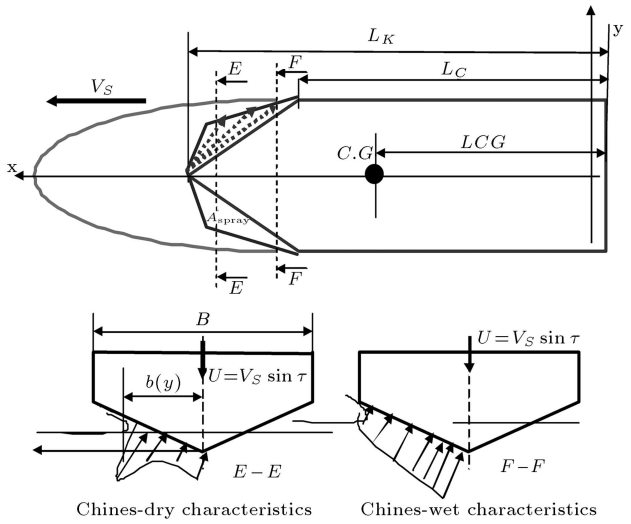


**Figure 4.** Scheme of the spray and its flow.

specified in Figure 4. In the present paper, the spray resistance and lift generated by the spray is estimated separately by the following equations:

$$L_{\text{Spray}} = P_S A_{\text{Spray}} \cos\tau,$$
$$R_{\text{Spray}} = P_S A_{\text{Spray}} \sin\tau. \tag{26}$$

### Hydrodynamic Pressure and Forces

The pressure on the hull surface is calculated by Bernoulli's equation as follows:

$$\frac{P}{\rho} = -gz - \frac{1}{2}\nabla\phi \cdot \nabla\phi$$
$$= -\left(gz + \left(\frac{1}{2}\nabla\phi - \vec{V}_S\right).\nabla\phi\right), \tag{27}$$

$$P = -\rho g h_z + 0.5\rho\left(2\vec{V}_S.\vec{v}_t - \vec{v}_t.\vec{v}_t\right). \tag{28}$$

The first term in the right part of Equation 28 is the hydrostatic pressure, $P_h$, and $h_z$ is immersion of the hull surface position. The second term is the dynamic part of pressure, $P_d$, which is generated by the induced velocity. The hydrodynamic lift forces ($L_d$), buoyant force ($L_s$) and induced resistance ($R_i$) acting on the hull can be obtained by integrating the pressure over the entire wetted surface:

$$L_d = 0.5\ \rho \int_{S_B} \left(2\vec{V}_S.\vec{v}_t - \vec{v}_t.\vec{v}_t\right) n_z dS,$$

$$L_s = \int_{S_B} \rho g h_z dS,$$

$$R_i = 0.5\ \rho \int_{S_B} \left(2\vec{V}_S.\vec{v}_t - \vec{v}_t.\vec{v}_t\right) n_x dS, \tag{29}$$

where $\vec{n}(n_x, n_y, n_z)$ is the outward unit normal vector on the wetted body surface.

### Resistance and Lift

The total resistance ($R_T$) of the non-planing craft is the summation of the two components, i.e. wave-making resistance $R_W$ and viscous resistance $R_V$:

$$R_{T_{(\text{non - planing})}} = R_W + R_V. \tag{30}$$

$R_W$ is determined from normal pressure acting on the wetted hull surface. This component is a function of the Froude number, but $R_V$ is the tangential force acting on the wetted hull surface and depends on the Reynolds number. The first part of the paper is focused on determination of the pressure and wave-making resistance.

The total resistance ($R_T$) of the planing craft is the summation of the three components, i.e. spray resistance, $R_{\text{Spray}}$, induced resistance, $R_i$, and frictional resistance, $R_F$.

$$R_{T_{(\text{planing})}} = R_S + R_i + R_F, \tag{31}$$

where $R_F$ is determined by the ITTC empirical formula [27]. $R_{\text{Spray}}$ and $R_i$ are obtained by Equations 26 and 29, respectively.

For the planing craft, the volumetric Froude number is a very important parameter that is defined as:

$$Fn_\nabla = \frac{V_S}{\sqrt{g\nabla^{1/3}}}, \tag{32}$$

where $\nabla$ is the volume displacement. Mass displacement is defined by $\Delta(=\rho\nabla)$ which is equal to the weight of the craft. For the planing craft, when the speed increases ($Fn_\nabla > 2$), the hull of the craft rises up and goes into the planing condition, which causes the wetted surface to diminish and the frictional resistance to come down. On the planing condition, the weight of the craft is supported mostly by hydrodynamic force (lift) and less by hydrostatic force (buoyant). In general, the weight of the craft is supported by the lift and the buoyant ($\Delta = W$ = Lift + Buoyant). Under a displacement condition (low speed), the weight is equal to the buoyant ($\Delta = W$ = Buoyant), but under a full planing condition (high speed), the weight is equal to lift ($\Delta = W \approx$ Lift).

A number of non-dimensional coefficients of pressure ($C_P$), hydrodynamic lift ($C_{L_d}$), buoyant ($C_{L_s}$) and

induced resistance ($C_{R_i}$) are used. They are defined as:

$$C_P = \frac{P}{\frac{1}{2}\rho V_S^2}, \qquad C_{L_d} = \frac{L_d}{1/2\rho V_S^2 S_B},$$

$$C_{L_s} = \frac{L_s}{1/2\rho V_S^2 S_B}, \qquad C_{R_i} = \frac{R_i}{1/2\rho V_S^2 S_B}, \tag{33}$$

where $S_B$ is the wetted body surface.

The wave profile can be obtained by the Taylor series expansion as:

$$\zeta = -\frac{V_S}{g}\frac{\partial \phi}{\partial x} \quad \text{on} \quad S_F. \tag{34}$$

After calculating velocity $\nabla\Phi(=\vec{V}_S+\nabla\phi)$, the pressure coefficient can be evaluated as:

$$C_P = 1 - \left(\frac{\nabla\Phi}{V_S}\right)^2 = 1 - \left(1 - \frac{\nabla\phi}{V_S}\right)^2. \tag{35}$$

Now, including the waterline integral, the wave-making coefficient ($C_W$) can be obtained as:

$$C_W = -\frac{\rho V_S^2 \int\limits_{S_B} C_P n_x dS + \rho g \oint\limits_{WL} \zeta^2 n_x dl}{\rho S_B V_S^2}. \tag{36}$$

## NUMERICAL RESULTS AND DISCUSSION

### Non-Planing Hull

The Wigley model is a mathematical displacement (non-planing) model and is popular in ship hydrodynamics. Many experimental and numerical results can be found in the literature for this model. We employed this model to compare numerical results at low Froude numbers. The standard Wigley hull is a mathematical hull form, the geometric surface of which can be defined as:

$$y = \pm\frac{B}{2}\left[1 - \left(\frac{2x}{L}\right)^2\right]\left[1 - \left(\frac{z}{T}\right)^2\right], \tag{37}$$

where $L$ is the hull length, $B$ the full hull beam and $T$ the hull draft. For the standard Wigley hull used in this computation, the length-to-beam ratio, $L/B$, is 10 and the beam-to-draft ratio, $B/T$, is 1.6. Since the body is symmetric, one-half of the computational domain is used for numerical treatment. The elements from one hull length upstream to 2.5 hull lengths downstream, cover the free surface domain. The transverse extension of the free surface is about 1.6 hull length. The number of elements on the hull and free surfaces are taken as being 25 × 7 and 104 × 18, respectively. A four-point upstream difference operator is used in both longitudinal and transverse directions to advent disturbances in the downstream direction.

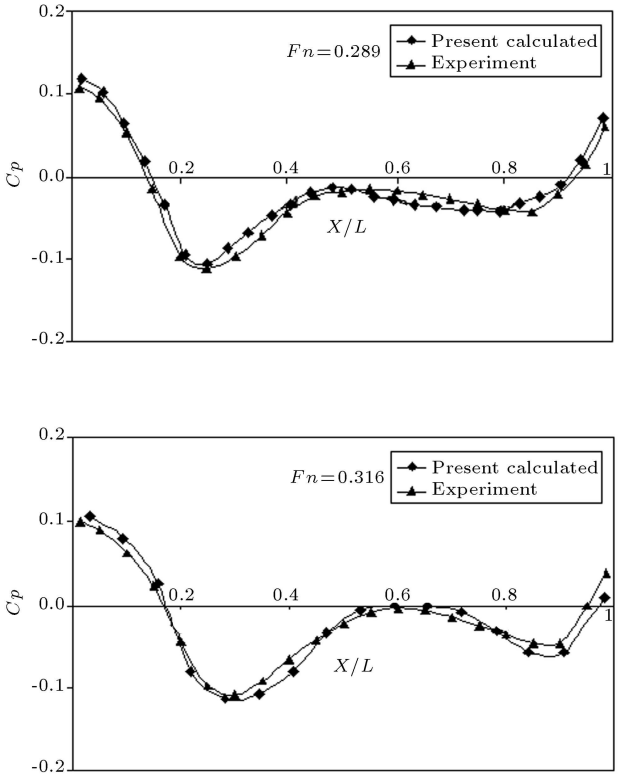


**Figure 5.** Comparison of pressure distribution along a Wigley hull at $Fn = 0.289, 0.316$.

Figure 5 shows a comparison of the pressure distribution along the Wigley hull for various Froude numbers, 0.289 and 0.316. It is found that the positive pressure values are concentrated on the small areas in the vicinity of the bow and the stern of the hull, and the negative pressure values are occurred on the rest of the hull.

Figure 6 presents comparisons of the wave elevations along the hull between the experimental measurements and the numerical results from the current solutions for Froude numbers of 0.267 and 0.316, respectively. The experimental measurements are for a model-fixed Wigley hull and given in [28]. The wave elevations along the hull have satisfactory agreement with the experimental measurements. In particular, at all Froude numbers, they completely approach the experimental data.

The prediction of the wave profile and wave pattern is very valuable in hull optimization, particularly in designing the ends of non-planing hulls. The computed perspective wave patterns view and free surface contours for the standard Wigley hull, at Froude number of 0.25, are shown in Figure 7. This is a three-dimensional view of the free surface profiles, and elevation of the free surface is clearly observed. The bow and stern wave systems, both containing the divergent and transverse wave patterns, are in good agreement with the Kelvin wave pattern. There

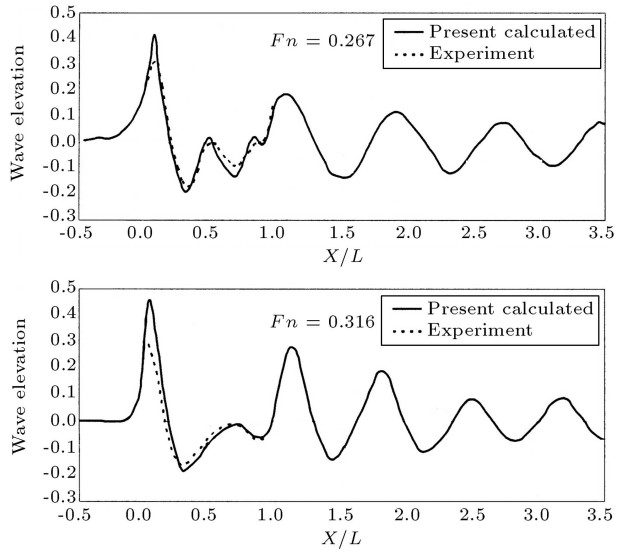


**Figure 6.** Comparison of wave elevation along Wigley hull at $Fn = 0.267, 0.316$.

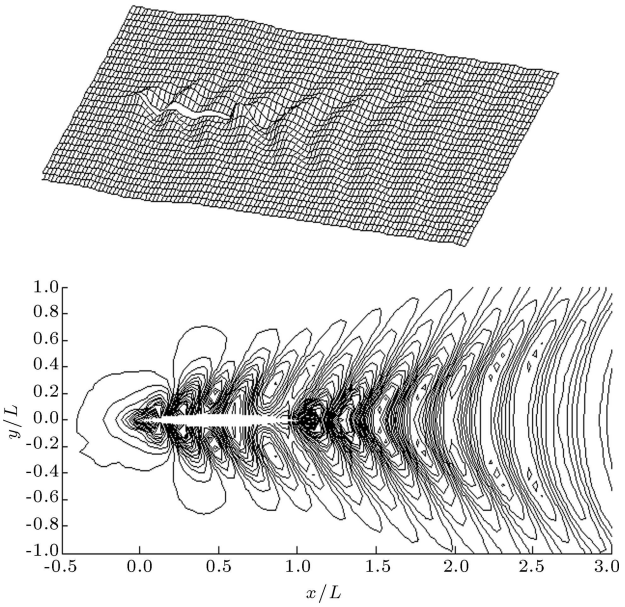


**Figure 7.** Free surface deformation and wave contours along Wigley hull at $Fn = 0.25$.

are no wave reflections at the side- and downstream-boundaries, since they are open boundaries for the computational domain. In Figure 8, the predicted values of wave resistance are compared with those of experiments [7]. The wave resistance curve shows a compatible variation with respect to the Froude number, and is consistent with experimental measurements.

## Planing Hull

In order to validate the numerical method for planing hulls, a planing flat plate is selected. Figure 9 shows the mesh arrangements on a planing flat plate. The flat

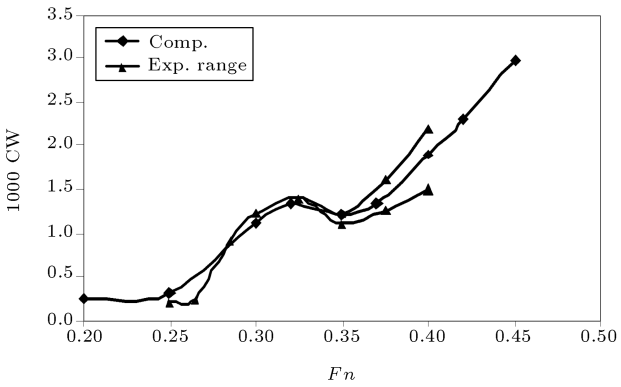


**Figure 8.** Comparison of the wave-making resistance of the Wigley hull.

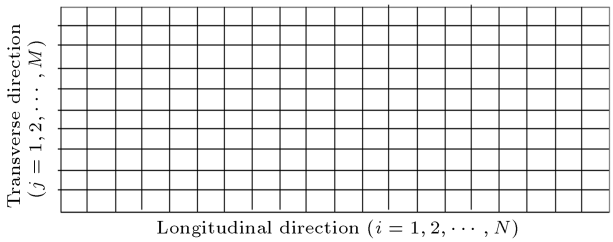


**Figure 9.** Mesh arrangements on planing flat plate ($N = 20, M = 10, L/B = 2.0$).

plate with $L/B = 2$ is discretized into 200 elements ($20 \times 10$) and the free surface is also discretized into 1800 elements ($60 \times 30$). Numerical results show that the number of given elements are enough for a flat plate and give a fairly converged solution. The pressure distribution on the center line of the hull is shown in Figures 10 and 11 for $Fn = 2.24$ ($F_n = V_S/\sqrt{Lg}$) and $L/B = 1$, $L/B = 2$, respectively. It is shown that the results of the present computations are in good agreement with other researcher's numerical results [20].

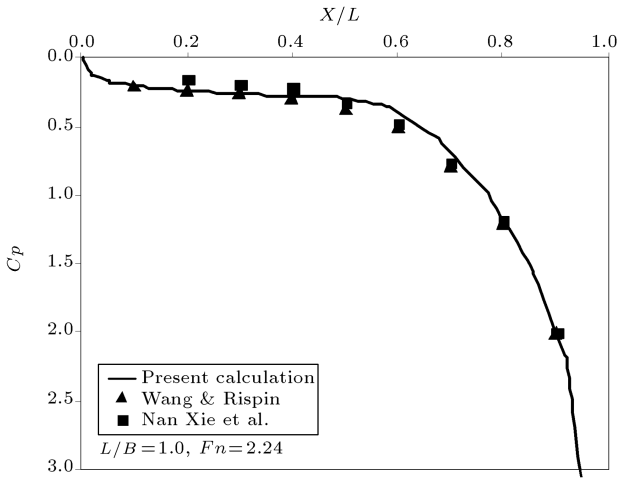


**Figure 10.** Comparison of pressure distribution on planing flat plate at center line ($L/B = 1, Fn = 2.24$).

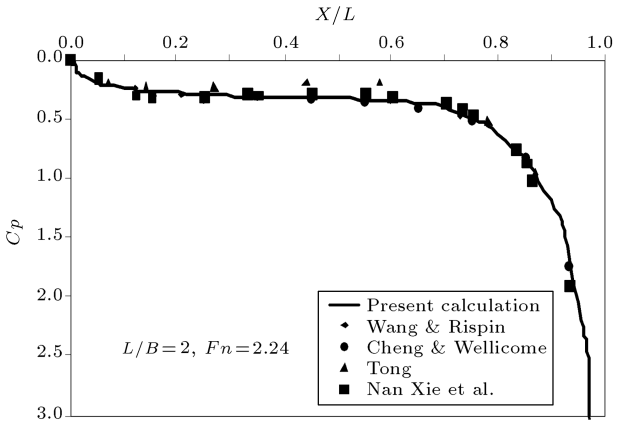


**Figure 11.** Comparison of pressure distribution on planing flat plate at center line ($L/B = 2, Fn = 2.24$).

The planing hull model 4666 is chosen to validate the numerical calculations. This planing hull has length-beam ratio 3.06, length 21.5 m, displacement $\Delta$ (or weight $= W$) 45 tones and mean deadrise angle 12.5 degree. Its body plan is illustrated in Figure 12. The hull is running with a steady forward motion in calm water at various volumetric Froude numbers from 1 to 6. The hydrodynamic pressure produced on the bottom of the body is calculated at various speeds, using a potential flow based boundary element method. At fully-planing speed, the hydrodynamic lift should be almost the same as the weight of the hull. When the speed increases, the hull will rise up and a new draft can be read. Therefore, due to different wetted surfaces, a new mesh system should be generated on the wetted surface for each speed. Under the semi-planing condition, the spatial technique was applied to obtain the draft at each speed.

Generation of accurate coordinates for each element on the body surface is more important in the BEM. A rough element division of the surface will affect the results of the pressure distribution. Then, it needs to have a smoother surface with a high precision interpolation for coordinates of the planing hull. In this case, the body is divided into a number of small quadrilateral elements. Figure 13 shows the mesh surface of the model. The model mesh shown in this figure is generated from the keel line to the chine line.

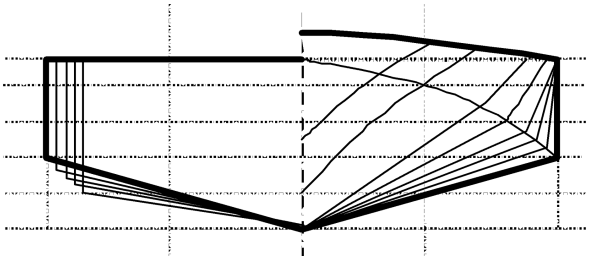

**Figure 12.** Body plan of the planing hull model 4666.

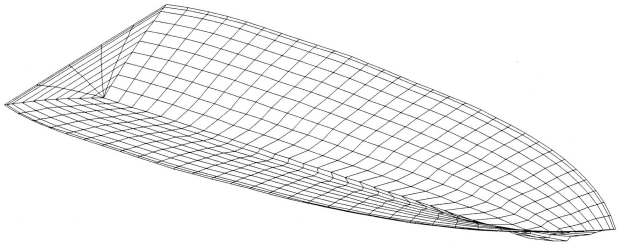

**Figure 13.** Mesh surface of the planing hull model 4666 (from bottom view).

The side is not included in this mesh surface, because it does not affect the hydrodynamic force as well as the spray force. In the calculations, the number of elements in longitudinal ($N_L$) and transverse ($N_T$) directions are considered 30 and 20, respectively. In total, 600 to 650 (depends on the transom wetted surface) elements on the hull surface plus 1800 elements on the free surface have been coordinated in the computations. The transom at the stern needs special treatment to assure the continuity of the normal vector on the body surface. For a volumetric Froude number greater than approximately 2.5, the flow separates from the transom and dry conditions are imposed.

Hydrodynamic pressure is computed by the induced velocity on the bottom of the planing hull. Figures 14 and 16 show the pressure distribution defined in Equation 31, which includes both hydrodynamic and hydrostatics terms for two volumetric Froude numbers of 3.35 and 5.0 at various longitudes strip-wise from bow to stern ($x/L$=0 is at stern).

The calculated longitudinal variation of the hydrodynamic and hydrostatic (buoyancy) components of the sectional lift coefficient are shown in Figures 15 and 17 for two speeds obtained by corresponding pressure.

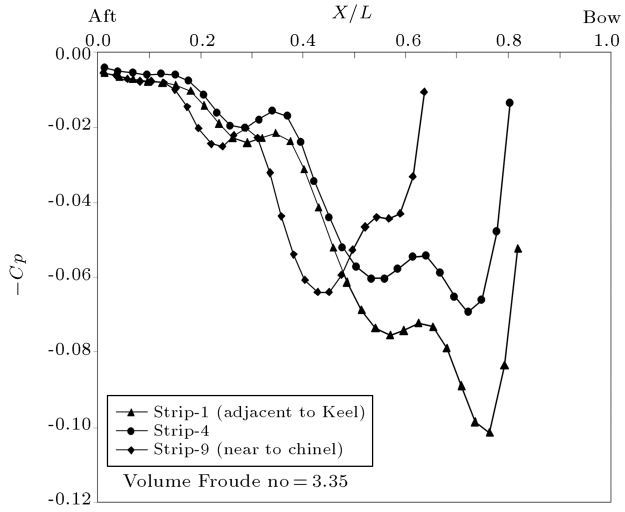


**Figure 14.** Distribution of pressure coefficient at various longitudinal strip-wise, $Fn_\nabla = 3.35$ for planing hull model 4666.

As can be seen from these figures, if the Froude number is increased, the buoyant lift coefficient decreases, while the hydrodynamic lift coefficient grows significantly. Figure 18 shows variations of the hydrodynamic lift coefficient as a function of volumetric Froude number. It is shown that when the volumetric Froude number exceeds 3.5, the hull is running to be fully in a planing condition and the lift is nearly the same as the weight of the hull.

The hull is raised up due to hydrodynamic pressure, so the physical condition of the hull is changed at various speeds. The wetted length and trim are changed. When the speed increases, the wetted length-beam ratio ($\lambda = L_w/B$) diminishes as shown in Figure 19. The center of pressure is almost constant and equals 6.4 m from the transom at all speeds ($x_{CP} = 6.4$). The craft is stable if the longitudinal center of gravity is located on the center of pressure ($x_{CP} = x_{CG}$). Otherwise, the craft crops up the pitching and longitudinal instability, which is out of range of the present research. We considered that the craft is moving with constant speed (steady condition),

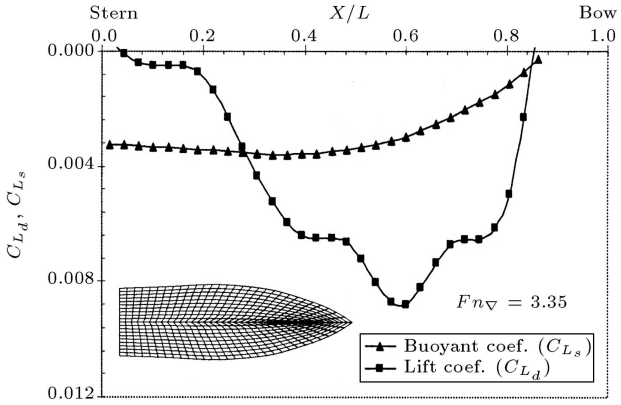


**Figure 15.** Distribution of buoyant and hydrodynamic lift coefficient, $Fn_\nabla = 3.35$ for planing hull model 4666.

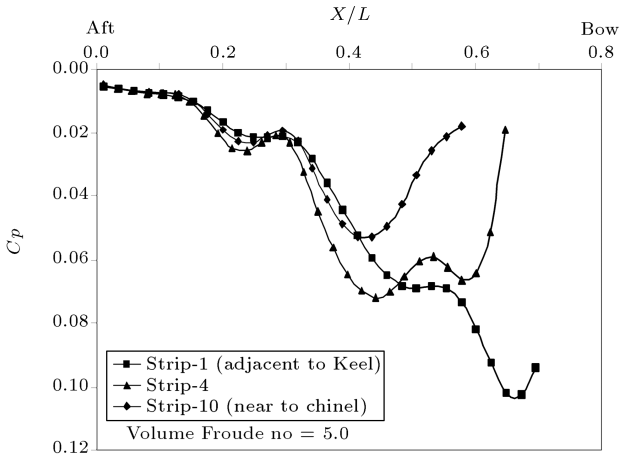


**Figure 16.** Distribution of pressure coefficient at various longitudinal strip-wise, $Fn_\nabla = 5.0$ for planing hull model 4666.

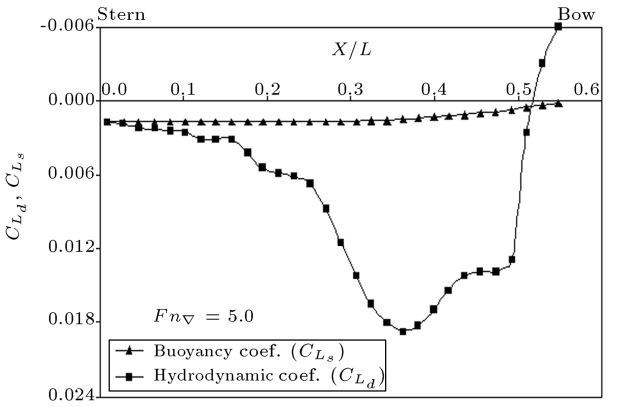


**Figure 17.** Distribution of buoyant and hydrodynamic lift coefficient, $Fn_\nabla = 5.0$ for planing hull model 4666.

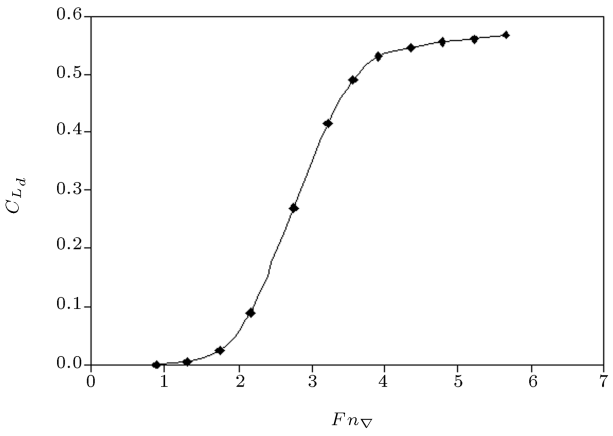


**Figure 18.** Hydrodynamic lift coefficient in terms of Froude numbers for planing hull model 4666.

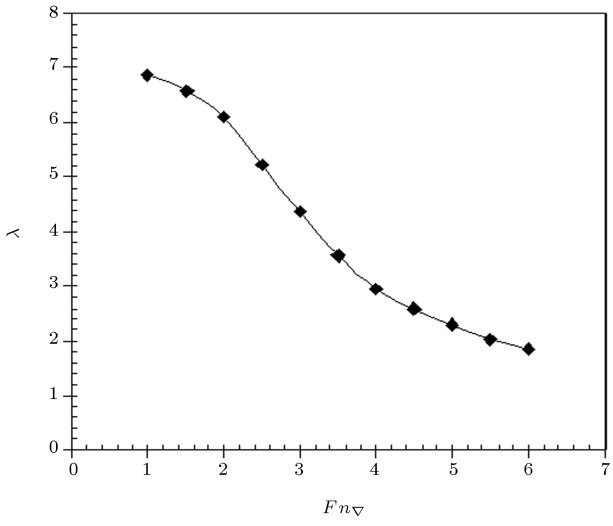


**Figure 19.** Wetted length-beam ratio ($\lambda = L_w/B$) in terms of Froude numbers for planing hull model 4666.

while longitudinal instability may occur at an unsteady condition and would need new aspects of numerical evaluation.

The calculated trim angle is given in Figure 20 as a function of the Froude number. This figure provides trim comparison, which is slightly in good agreement with experimental data [1]. The maximum trim angle is between 5 to 6 degree in experiment and numerical results, respectively. When the speed increases, the trim angle diminishes. The trim angle is about 1.5 to 2 degree at $Fn_\nabla = 6.0$. The pressure distribution on the bottom of the prismatic planing hull is shown in Figure 21. It is obvious that high pressure is generated at the bow and low pressure occurs at the stern. The resistance-weight ratio components at various volumetric Froude numbers are presented in Figures 22. It is found that the resistance curve has a primary hump at around $Fn_\nabla = 1.7$ and a primary hallow (take-off point) at around $Fn_\nabla = 3$, increasing moderately when the speed increases. The computed resistance-weight ratio shows favorable agreement with the experimentally determined values.

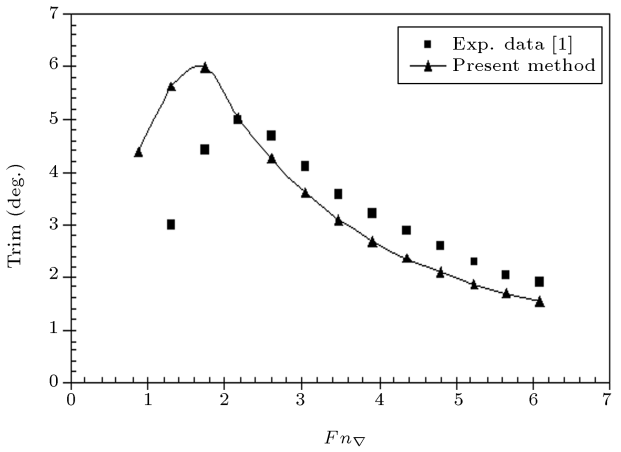


**Figure 20.** Comparison of trim angle in terms of Froude numbers for planing hull model 4666.

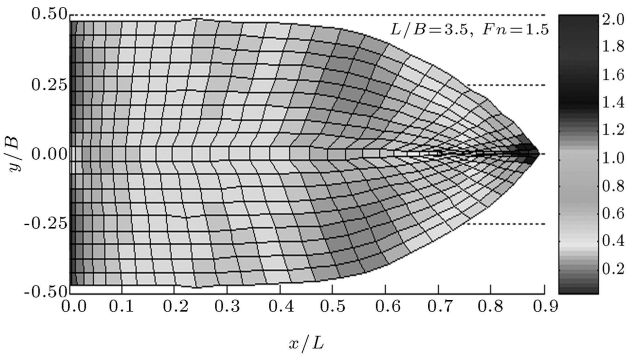


**Figure 21.** Pressure distribution on the bottom of the planing hull at $Fn_\nabla = 3.7$ or $Fn = 1.5$.

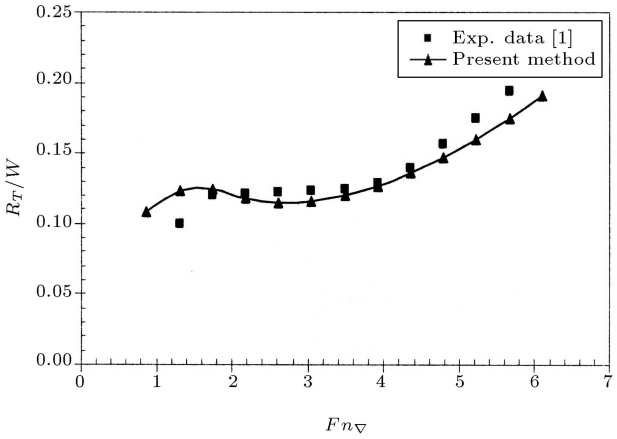


**Figure 22.** Resistance-weight ratio ($R_T/W$) in terms of Froude numbers for planing hull model 4666.

## CONCLUSIONS

This paper employed a potential based boundary element method to analyze the hydrodynamic characteristics of three-dimensional planing and non-planing hull surfaces. A special technique is practically used for the spray resistance. Two hull forms, i.e. a non-planing model (Wigley) and a planing hull, have been selected to compare computation results with analytical or experimental data. Generally, the following conclusions can be drawn:

- Comparison of calculated pressure distributions and wave elevation; the wave resistance of the Wigley hull are well in agreement with experimental data.
- An additional boundary condition (like the Kutta condition) is required for a planing hull. It is physically important to reach the pressure that is atmospheric pressure at the transom. This is completely different regarding a non-planing hull.
- The effects of varying the Froude number are examined for a planing hull. It is found that the hydrodynamic lift to weight ratio ($L/W$) for the planing hull is about 60% and 85% at $Fn_\nabla = 3.0$ and $Fn_\nabla = 5.0$, respectively.
- The center of pressure is almost constant at all speeds and is placed at the center of gravity ($x_{CP} = x_{CG} = 6.4$ m). Otherwise, pitching moment and longitudinal instability may occur.

Our future plan is to work on a continuous numerical calculation including the spray term.

## REFERENCES

1. Clement, E.P and Blount, D.L. "Resistance tests of systematic series of planing hull forms", *SNAME Transaction*, **71**, pp. 491-579 (1963).

2. Insel, M. "Advanced marine vehicles lectures notebook", Dept. of naval architecture and ocean engineering, Istanbul Technical University (2000).

3. Wehausen, J.V. *The Wave Resistance of Ships, Advances in Applied Mechanics*, Academic Press Inc., Elsevier Ltd (1970).

4. Noblesse, F. and McCarthy, J.H., Editors, *Proceedings of the Second DTNSRDC Workshop on Ship Wave-Resistance Computations*, Bethesda, MD, USA (1983).

5. Dawson, C.W. "A practical computer method for solving ship-wave problems", *Proceedings of the 2nd International Conference on Numerical Ship Hydrodynamics*, USA (1977).

6. Tong, J. "A finite element approach to planing problem", PhD Thesis, University of Southampton (1989).

7. Nakos, D.E. and Sclavounos, P.D. "Kelvin wakes and wave resistance of cruiser- and transom-stern ships", *Journal of Ship Research*, **38**, pp. 9-29 (1994).

8. Bal, S. "Prediction of wave pattern and wave resistance of surface piercing bodies by a boundary element method", *International Journal of Numerical Methods in Fluids*, **56**(3), pp. 305-329 (2008).

9. Tarafdera. M.S. and Suzuki, K. "Computation of wave-making resistance of a catamaran in deep water using a potential-based panel method", *Ocean Engineering*, **34**, pp. 1892-1900 (2007).

10. Xia, F. "Numerical calculation of ship flows with special emphasis on the free-surface potential flow", PhD Dissertation, Chalmers University of Technology, Sweden (1986).

11. Cao, Y., Schultz, W.W. and Beck, R.F. "Three dimensional desingularized boundary integral methods for potential problems", *International Journal of Numerical Method in Fluids*, **12**, pp. 785-803 (1991).

12. Bassanini, P., Bulgarelli, U., Campana, E. and Lalli, F. "The wave resistance problem in a boundary integral formulation", *Surv. Math. Ind.*, **4**, pp. 151-194 (1994).

13. Savitsky, D. "Hydrodynamic design of planing hulls, *Marine Technology*, **1**(1), pp. 71-95 (1964).

14. Katayama, T., Hayashita, S., Suzuki, K. and Ikeda, Y. "Development of resistance test for high-speed planing hull using very small model-scale effects on resistance force-proceedings of Asia Pacific workshop on hydrodynamics", pp. 7-14 (2002).

15. Lai, C. and Troesch, A.W. "A vortex lattice method for high speed planing", *International Journal of Numerical Method in Fluids*, **22**, pp. 495-513 (1996).

16. Zhao, R., Faltinsen, O.M and Haslum, H.A. "A simplified nonlinear analysis of a high- speed planing hull in calm water", *Proceedings, 4th Int. Conf. on Fast Sea Transportation*, Australia (1997).

17. Savander, B.R., Scorpio, S.M. and Taylor, R.K. "Steady hydrodynamic of planing surface", *J. of Ship Research*, **46**(4), pp. 248-279 (2002).

18. Xie, N., Vassalos, D., Jasionowski, A. "A study of hydrodynamics of three-dimensional planing surface", *J. of Ocean Engineering*, **32**, pp. 1539-1555 (2005).

19. Rahmanian, A. "Computational analysis of planing hull using BEM", Master Thesis, Department of Marine Technology, Amirkabir University of Technology (2004).

20. Wang, D.P. and Rispin, P. "Three-dimensional planing at high Froude number", *Journal of Ship Research*, **15**(3), pp. 221-230 (1971).

21. Cheng, X., and Wellicome, J.F. "Study of planing hydrodynamics using strips of transversely variable pressure", *J. of Ship Research*, **38**(2), pp. 30-41 (1994).

22. Sadathosseini, S.H., Mousaviraad, S.M., Firoozabadi, B. and Ahmadi, G. "Numerical simulation of free-surface waves and wave induced separation", *Scientia Iranica*, **15**(3), pp. 323-331 (2008).

23. Ghassemi, H. and Ghiasi, M. "A combined method for the hydrodynamic characteristics of planing crafts", *Ocean Engineering*, **35**, pp. 310-322 (2008).

24. Ghassemi, H., Kohansal, A.R. and Ghamari, I. "Nonlinear free surface flows due to the lifting and non-lifting moving bodies", *17th Annual (International) Conference on Mechanical Engineering* - ISME2009, Tehran, Iran (May 2009).

25. Savitsky, D., DeLorme, M.F. and Raju, D. "Inclusion of whisker spray drag in performance prediction method for high-speed planing hulls", *Journal of Marine Technology*, **44**, pp. 35-56 (2007).

26. Bowles, B.J. and Denny, S.B. "Water surface disturbance near the bow of high speed", *Hard Chine Hull Forms, International Conference on Fast Sea Transportation*, (FAST) St. Petersburg, Russia (2005).

27. Faltinsen, O.M., *Hydrodynamics of High-Speed Marine Vehicles New York*, Cambridge University Press (2005).

28. Kajitani, H., Miyata, H., Ikehata, M., Tanaka, H. and Adachi, H. "Summary of the cooperative experiment on wigley parabolic model in Japan", *Proceedings of the Workshop on Ship Wave Resistance Computations*, pp. 5-35 (1983).